LETTER

doi:10.1038/nature13799

Centennial-scale changes in the global carbon cycle during the last deglaciation

Shaun A. Marcott[1,2], Thomas K. Bauska[1], Christo Buizert[1], Eric J. Steig[3], Julia L. Rosen[1], Kurt M. Cuffey[4], T. J. Fudge[3], Jeffery P. Severinghaus[5], Jinho Ahn[6], Michael L. Kalk[1], Joseph R. McConnell[7], Todd Sowers[8], Kendrick C. Taylor[7], James W. C. White[9] & Edward J. Brook[1]

Global climate and the concentration of atmospheric carbon dioxide (CO_2) are correlated over recent glacial cycles[1,2]. The combination of processes responsible for a rise in atmospheric CO_2 at the last glacial termination[1,3] (23,000 to 9,000 years ago), however, remains uncertain[1–3]. Establishing the timing and rate of CO_2 changes in the past provides critical insight into the mechanisms that influence the carbon cycle and helps put present and future anthropogenic emissions in context. Here we present CO_2 and methane (CH_4) records of the last deglaciation from a new high-accumulation West Antarctic ice core with unprecedented temporal resolution and precise chronology. We show that although low-frequency CO_2 variations parallel changes in Antarctic temperature, abrupt CO_2 changes occur that have a clear relationship with abrupt climate changes in the Northern Hemisphere. A significant proportion of the direct radiative forcing associated with the rise in atmospheric CO_2 occurred in three sudden steps, each of 10 to 15 parts per million. Every step took place in less than two centuries and was followed by no notable change in atmospheric CO_2 for about 1,000 to 1,500 years. Slow, millennial-scale ventilation of Southern Ocean CO_2-rich, deep-ocean water masses is thought to have been fundamental to the rise in atmospheric CO_2 associated with the glacial termination[4], given the strong covariance of CO_2 levels and Antarctic temperatures[5]. Our data establish a contribution from an abrupt, centennial-scale mode of CO_2 variability that is not directly related to Antarctic temperature. We suggest that processes operating on centennial timescales, probably involving the Atlantic meridional overturning circulation, seem to be influencing global carbon-cycle dynamics and are at present not widely considered in Earth system models.

Ice cores from Greenland[6,7] provide unique records of rapid climate events of the past 120 kyr. However, because of relatively high concentrations of impurities[8], Greenlandic ice cores do not provide reliable atmospheric CO_2 records. Antarctic ice cores, which contain an order-of-magnitude fewer impurities, provide reliable records[8], but existing data from the deglacial period from Antarctica either provide only low temporal resolution[9] or are of relatively low precision[10].

The West Antarctic Ice Sheet Divide ice core (WDC) (79.467° S, 112.085° W, 1,766 m above sea level) was drilled to a depth of 3,405 m in 2011 and spans the past ~68 kyr. At present, the site has a mean annual snow accumulation of 22 cm ice equivalent per year and a surface temperature of −30 °C. Annual layer counting to 2,800 m depth (~30 kyr ago) provides a very accurate timescale for comparison with data from other archives[11]. The difference in age (Δage) between the ice and the gas trapped within it, which is critical for developing a gas-age chronology, is 205 ± 10 yr at present and was 525 ± 100 yr at the last glacial maximum (LGM) (Extended Data Fig. 1). Given the high accumulation at the site, minimal smoothing due to gas transport and gradual occlusion, and precise chronological constraints, WDC is the best Antarctic analogue to central Greenlandic deep ice cores, with a substantially better-dated gas chronology during the glacial period, and is able to resolve atmospheric CO_2 at sub-centennial resolution.

We exploit the unique aspects of WDC to reconstruct atmospheric CO_2 and CH_4 concentrations at high resolution over the last deglaciation. The atmospheric CH_4 record is important in this context because CH_4 varies in phase with rapid Greenlandic climate changes during the deglaciation and therefore provides a means of synchronizing our Antarctic record with Northern Hemisphere climate[12]. Atmospheric CH_4 is primarily produced by land-based sources, principally tropical and boreal wetlands[13] where emissions are driven by changes in temperature and hydrology, and CH_4 therefore serves as an indicator of processes in the terrestrial biosphere.

The WDC deglacial CO_2 record is characterized by a long-term ~80 p.p.m. increase, similar to other cores[9,14], which begins at 18.1 kyr ago, occurs in several discrete steps throughout the deglacial transition, and ends 7 kyr later, during the early Holocene epoch. Given the precise WDC chronology, the phasing of CO_2 changes with respect to Antarctic and global temperature[2] can be more precisely evaluated. The timing of the initial deglacial CO_2 rise leads the initial rise in global temperature[2] (17.2 kyr ago) by several centuries, and continues to lead across the entire termination (Extended Data Fig. 7). The timing of the initial CO_2 rise is consistent with the newest gas chronology of EPICA Dome C[5] (EDC), but more highly resolved and precise given the smaller gas-age uncertainty in WDC than in EDC (Extended Data 4). The WDC methane record shows in detail the abrupt changes at the onset of the Bølling–Allerød and Younger Dryas stadials and the start of the Holocene. We observe a smaller, but prominent, methane excursion at 16.3 kyr ago not previously reported from other records (Fig. 1). Our record also resolves the beginning of the deglacial methane rise at 17.8 kyr ago (Extended Data Table 1).

The WDC CO_2 record demonstrates that CO_2 varied in three distinct modes during the deglaciation. The first mode is relatively gradual change (~10 p.p.m. kyr^{-1}): such changes in CO_2 began at 18.1 and 13.0 kyr ago and were broadly coincident with a reduction in the strength of the Atlantic meridional overturning circulation (AMOC; Fig. 2i), a cold North Atlantic[2] and warming in the Southern Hemisphere[2]. The second mode is rapid increase: 10–15 p.p.m. increases in CO_2 occurred in three short (100–200 yr) intervals at 16.3, 14.8 and 11.7 kyr ago, the latter two at times of rapid resumption of the AMOC and warming in the Northern Hemisphere. The rapid changes at 14.8 and 11.7 kyr ago were first noted at EDC[9,14], but the magnitude, duration and timing are now more fully resolved because of the unique site conditions at WDC. The third mode is no change in atmospheric CO_2. These apparent plateaus in the WDC CO_2 record lasted for 1,000–1,500 yr and occurred directly after the rapid, century-scale increases.

[1]College of Earth, Ocean, and Atmospheric Sciences, Oregon State University, Corvallis, Oregon 97331, USA. [2]Department of Geoscience, University of Wisconsin-Madison, Madison, Wisconsin 53706, USA. [3]Department of Earth and Space Sciences, University of Washington, Seattle, Washington 98195, USA. [4]Department of Geography, University of California, Berkeley, California 94720, USA. [5]Scripps Institution of Oceanography, University of California, San Diego, California 92037, USA. [6]School of Earth and Environmental Sciences, Seoul National University, Seoul 151-742, South Korea. [7]Desert Research Institute, Nevada System of Higher Education, Reno, Nevada 89512, USA. [8]Earth and Environmental Systems Institute, Pennsylvania State University, University Park, Pennsylvania 16802, USA. [9]INSTAAR, University of Colorado, Boulder, Colorado 80309, USA.

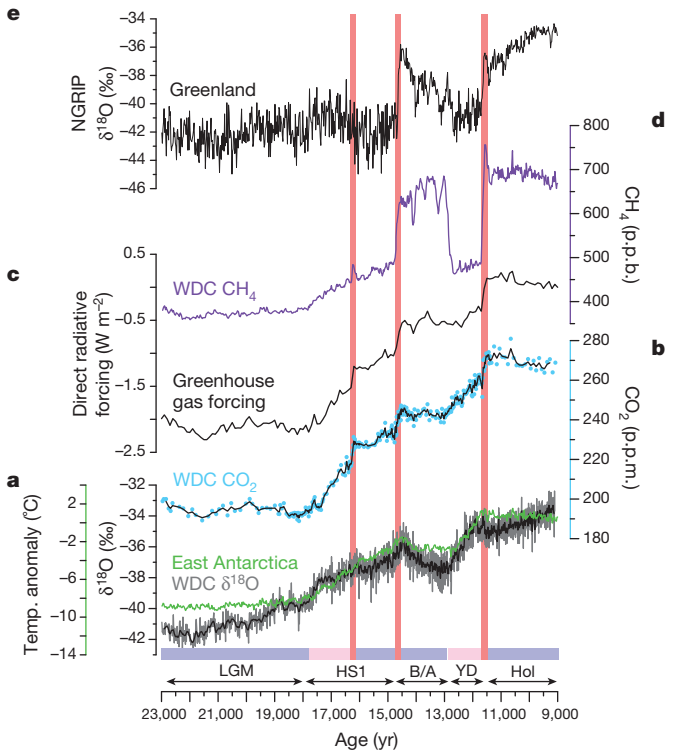

Figure 1 | Greenhouse gas and stable water isotope measurements from Antarctica and Greenland. **a**, Oxygen isotopes from WDC[11] (grey; black line is 11-point weighted average) and water-isotope-derived temperature composite from East Antarctica[5] (green). $\delta^{18}O = (^{18}O/^{16}O)_{sample}/(^{18}O/^{16}O)_{VSMOW} - 1$; VSMOW, Vienna Standard Mean Ocean Water. **b**, Atmospheric CO_2 concentrations (this study; black line is 5-point weighted average). **c**, Direct radiative forcing of CO_2, CH_4 and N_2O (ref. 31) using a simplified expression[32]. **d**, Atmospheric CH_4 concentrations (this study and ref. 11). **e**, Oxygen isotope measurements from the North Greenland Ice Project[6] (NGRIP). Coloured bands at bottom indicate times when CO_2 is stable (blue), slowly increasing (pink) or rapidly increasing (red), as described in the text. LGM, Last Glacial Maximum; HS1, Heinrich stadial 1 (~18.0–14.6 kyr ago); B/A, Bølling–Allerød; YD, Younger Dryas; Hol, Holocene.

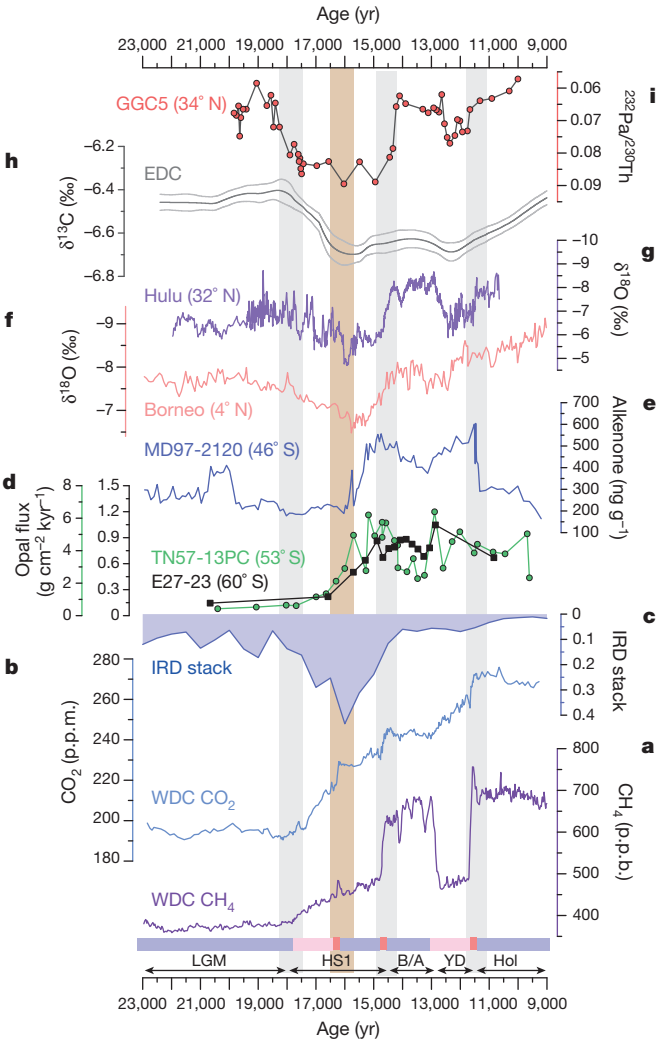

Figure 2 | WAIS Divide CO_2 and CH_4 data plotted against multiple environmental proxies. **a**, **b**, WAIS Divide CH_4 (**a**) and CO_2 (**b**). **c**, Iceberg discharge indices from the North Atlantic[23] (15-record composite; normalized units). IRD, ice-rafted debris. **d**, **e**, Biological flux proxies from the Southern Ocean[18] (**d**; TN57-13PC and E27-23) and off New Zealand[25] (**e**; MD97-2120). **f**, **g**, Precipitation indices in speleothem records from Borneo[26] (**f**) and Hulu[27] (**g**). **h**, Carbon isotopes of CO_2 (line with 1σ uncertainty band) from a multi-core composite[4] placed on an updated chronology[5]. $\delta^{13}C = (^{13}C/^{12}C)_{sample}/(^{13}C/^{12}C)_{VPDB} - 1$; VPDB, Vienna PeeDee Belemnite. **i**, An AMOC proxy[19] (GGC5). All age models that use radiocarbon dates were recalibrated with IntCal13 and updated (Supplementary Data). Coloured bands at bottom of plot indicate times when CO_2 is stable (blue), slowly increasing (pink) or rapidly increasing (red), as described in the text. The grey and brown bands denote the timing of notable climatic transitions (for example LGM to HS1).

The increase in CO_2 from glacial to interglacial states is typically explained by a combination of changes in deep-ocean ventilation, Antarctic sea-ice cover, ocean salinity and temperature, marine biological surface nutrient utilization, changes in ocean alkalinity, and carbonate compensation in the ocean[15]. These processes are generally thought to take place at millennial or longer timescales. However, our new observations from WDC demonstrate that in several instances the observed atmospheric CO_2 change was rapid, on centennial timescales; that the most rapid changes correlate in time with ice-rafted debris events in the North Atlantic or with abrupt changes in the AMOC (Fig. 2); and that the abrupt changes in CO_2 do not always have a centennial counterpart in the Antarctic $\delta^{18}O$ record (Fig. 1).

Given these new observations, we suggest that the AMOC had a critical role in the glacial–interglacial rise of atmospheric CO_2 and may have acted as a modulator of both the timing and the magnitude of CO_2 and CH_4 change during the last termination, either directly, through changes in ocean circulation, or indirectly, through the redistribution of heat and the associated climate response. Elements of this hypothesis have been outlined previously: a reduction in the AMOC is thought to cause increased overturning in the Southern Ocean, which allows CO_2 in the deep ocean to enter the ocean mixed layer more rapidly, where it can exchange with the atmosphere[16]. For methane, a cooling in the Northern Hemisphere resulting from a reduction in the AMOC and a southward expansion of sea-ice extent may have displaced the intertropical convergence zone southwards[17] resulting in decreased production of methane from mid- and low-latitude sources, and vice versa when the Northern Hemisphere warmed. Several studies have proposed other complementary mechanisms (see, for example, ref. 18) for the CO_2 changes across the last termination; here we guide the discussion with a simple working hypothesis that the AMOC had a critical role, either directly or indirectly, in the rise of atmospheric CO_2.

The gradual changes in CO_2 that begin at 18.1 and 13.0 kyr ago are accompanied by a reduction in the AMOC strength[19] and warming in Antarctica[11] (Figs 1 and 2). Like CO_2, methane begins to increase gradually at ~18 kyr ago (50 p.p.b. kyr^{-1}), yet at 13.0 kyr ago it is decoupled from CO_2 and instead decreases by 200 p.p.b. in two centuries before stabilizing during the Younger Dryas (Fig. 1). The CO_2 rise and abrupt CH_4 drop at 13 kyr ago are synchronous within the resolution of the data (20–60 yr), and both rise almost synchronously at 18 kyr ago (Extended Data Table 1), suggesting that a common forcing drives the

changes in both gases. Freshwater hosing experiments with a coupled atmosphere–ocean–biogeochemical model[20] show that atmospheric CO_2 begins to rise because of a decrease in the ocean carbon inventory due to a collapse in the AMOC, and continues rising until the AMOC resumes. The rate of CO_2 rise in the model[20] (25 p.p.m. in 1,700 yr) is similar to rates observed from WDC, and the hypothesis that CO_2 fluctuations are controlled by ocean circulation change is consistent with the timing of the AMOC reduction based on ocean proxies (Fig. 2). Two significant depletion events in stable carbon isotope ratios of CO_2 from a composite of multiple ice cores[4], by 0.3‰ and 0.1‰, are consistent with the source of the CO_2 rises at 18.1 and 13.0 kyr ago being from upwelling of respired carbon from the deep ocean (Fig. 2h).

The most abrupt changes in CO_2 during the last termination occur at 16.3, 14.8 and 11.7 kyr ago and are synchronous with abrupt increases in CH_4 within the 20–60 yr resolution of the data (Fig. 3). No relationship between the carbonate chemistry of the ice and CO_2 concentration is observed that would suggest *in situ* production of CO_2 as observed in Greenland[8] (Extended Data Fig. 2), and the sharp increases are resolved by multiple data points, each multiply replicated. Moreover, the WDC CO_2 record is consistent with results from the EDC ice core[5,9,14] after accounting for the greater smoothing of the EDC gas record by the increased diffusion in the firn and the gradual bubble closure characteristic of low-accumulation sites (Extended Data Fig. 5b). For all three of the abrupt CO_2 increases, the concomitant CH_4 rise is even more sudden, suggesting that the rate of the CO_2 increase in the WDC record is not limited by firn smoothing processes, but reflects the true atmospheric rate of change.

For the abrupt increases at 14.8 and 11.7 kyr ago, both CO_2 and CH_4 increased by ~13 p.p.m. and ~200 p.p.b., respectively, in 100–200 yr, and then remained at the new levels. For these two events, the increases are coincident with proxy evidence for an abrupt recovery of the AMOC and a rapid warming of the North Hemisphere as recorded by Greenlandic ice cores (Fig. 2). As previously noted, modelling suggests that slow increases in CO_2 can occur when the AMOC is reduced[20]. Conversely, similar modelling supports the hypothesis that a rapid resumption of the AMOC can result in an abrupt increase in atmospheric CO_2 and CH_4 through changes in carbon storage on land[21] and increased precipitation in wetland regions. Other modelling studies[22] suggest that the CO_2 increase at the onset of the Bølling warming could have been much higher given the large smoothing at EDC. Such an overshoot in CO_2 is not recorded at the Bølling onset at WDC, but smaller overshoots at 11.7 and 16.3 kyr ago do lend partial support to this mechanism.

At 16.3 kyr ago, CO_2 and CH_4 also abruptly increased by 12 p.p.m. and 50 p.p.b. in 100 yr, respectively, although the elevated methane levels were short lived (Fig. 3). However, unlike the changes at 14.8 and 11.7 kyr ago, these increases show no apparent evidence for an abrupt AMOC resumption or warming in the Northern Hemisphere. We propose that the abrupt rise in CO_2 at 16.3 kyr ago is directly related to an iceberg discharge event recorded in several ocean cores from the North Atlantic[23], which occurred while the AMOC was already reduced (Fig. 2c). One potential cause of the CO_2 increase at this time could be a southward shift in the position of the Southern Hemisphere westerlies[24], leading to increased ocean upwelling and outgassing of respiration-derived CO_2 (ref. 18). Other archives preserve geochemical signals attributed to the iceberg discharge event at 16.3 kyr ago, for instance an increase in upwelling in the Southern Ocean[18] (Fig. 2d) and off the coast of New Zealand[25] (Fig. 2e), drying in northern Borneo[26] (Fig. 2f), and an inferred sharp decrease in monsoon intensity in central China[27] (Fig. 2g). Cooling and drying of large regions of the globe may also be a consequence of iceberg discharge and freshwater input into the North Atlantic[28], which could have initiated a rapid release of carbon from land stocks[29].

The small increase in methane at the time of the CO_2 rise at 16.3 kyr ago is somewhat puzzling because a southward shift in the intertropical convergence zone related to an iceberg discharge event would be expected to suppress northern tropical sources of CH_4. However, observations from cave deposits suggest wetter conditions at southern equatorial sites during Heinrich stadials[26], which could compensate for reduced northern sources[27] and explain the small CH_4 increase.

Finally, the apparent plateaux in CO_2 concentration that occur directly after each of the abrupt CO_2 increases at 16.3, 14.8 and 11.7 kyr ago (Fig. 1) deserve explanation. These plateaux last for 1,000–1,500 yr, and the plateaux following the abrupt changes at 14.8 and 11.7 kyr ago are contemporaneous with reinvigorated AMOC[19], cooling in Antarctica[5] and a decreased north–south gradient in global temperature[2]. One possible explanation is stratification of the Southern Ocean, perhaps in response to large freshwater discharges from the Antarctic ice sheet[30], which would lead to a reduction in outgassing of CO_2 to the atmosphere through decreased exchange of deep water with the surface ocean and

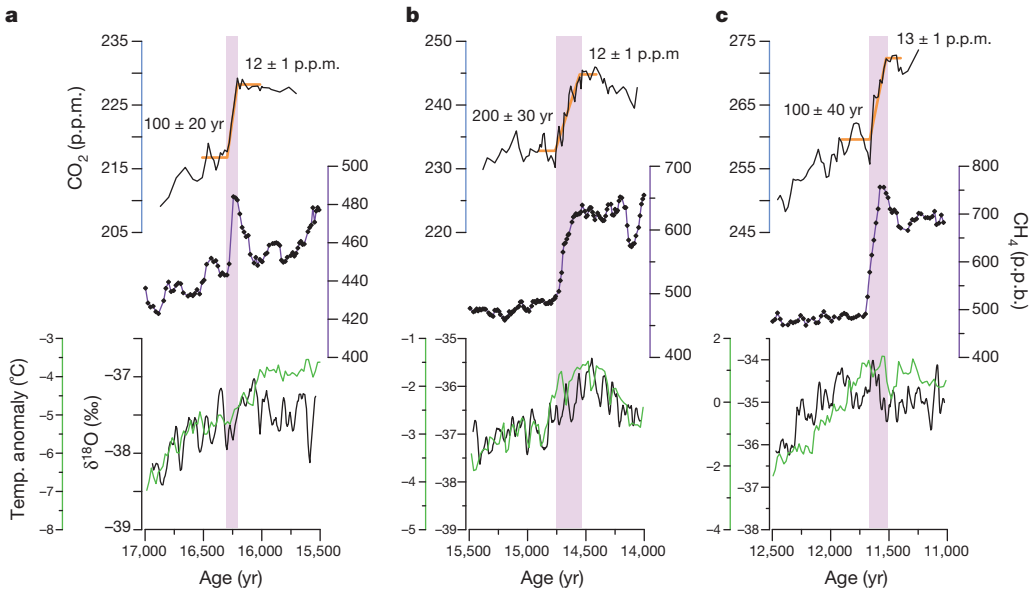

Figure 3 | Detailed view of greenhouse gas and stable isotope measurements from WDC. Oxygen isotope measurements from WDC[11] (black line is 11-point weighted average), water-isotope-derived temperature composite from East Antarctica[5] (green), and atmospheric CH_4 (purple) and CO_2 concentrations (black line is 5-point weighted average) across the abrupt CO_2 transition at 16.3 (**a**), 14.8 (**b**) and 11.7 kyr ago (**c**). Purple bands represent the durations of the abrupt CO_2 transition and orange lines show their magnitudes (durations and magnitudes also in parentheses; Extended Data Table 1).

atmosphere. Alternatively, the plateaux in CO_2 could be associated with the slow equilibration of atmospheric CO_2 with the ocean following the input of relatively large pulses of carbon during the CO_2 jumps (Extended Data Fig. 5), or uptake of atmospheric CO_2 by the slow regrowth of the terrestrial biosphere.

Our results provide evidence that the observed CO_2 rise during the last deglaciation was divided into two modes: a slow, millennial-scale mode that is closely linked to Antarctic temperature and associated with $\delta^{13}CO_2$ decreases (Fig. 2), suggestive of an oceanic origin; and a fast, centennial-scale mode that is closely linked to CH_4 and Northern Hemisphere climate, potentially controlled by AMOC strength and the associated climate teleconnections. Given that a large portion of the direct radiative CO_2 forcing during the glacial–interglacial rise occurred in approximately four centuries, future modelling and isotopic investigations should focus on explaining these abrupt CO_2 variations to further our understanding of the sensitivity of the carbon cycle under natural forcing.

Online Content Methods, along with any additional Extended Data display items and Source Data, are available in the online version of the paper; references unique to these sections appear only in the online paper.

Received 19 March; accepted 27 August 2014.

1. Petit, J. R. *et al.* Climate and atmospheric history of the last 420,000 years from the Vostok ice core, Antarctica. *Nature* **399,** 429–436 (1999).
2. Shakun, J. D. *et al.* Global warming preceded by increasing carbon dioxide concentrations during the last deglaciation. *Nature* **484,** 49–54 (2012).
3. Sigman, D. M. & Boyle, E. A. Glacial/interglacial variations in atmospheric carbon dioxide. *Nature* **407,** 859–869 (2000).
4. Schmitt, J. *et al.* Carbon isotope constraints on the deglacial CO_2 rise from ice cores. *Science* **336,** 711–714 (2012).
5. Parrenin, F. *et al.* Synchronous change of atmospheric CO_2 and Antarctic temperature during the last deglacial warming. *Science* **339,** 1060–1063 (2013).
6. North Greenland Ice Core Project members. High-resolution record of Northern Hemisphere climate extending into the last interglacial period. *Nature* **431,** 147–151 (2004).
7. Grootes, P. M., Stuiver, M., White, J. W. C., Johnsen, S. & Jouzel, J. Comparison of oxygen isotope records from the GISP2 and GRIP Greenland ice cores. *Nature* **366,** 552–554 (1993).
8. Smith, H. J., Wahlen, M., Mastroianni, D., Taylor, K. & Mayewski, P. The CO_2 concentration of air trapped in Greenland Ice Sheet Project 2 ice formed during periods of rapid climate change. *J. Geophys. Res.* **102,** 26577–26582 (1997).
9. Monnin, E. *et al.* Atmospheric CO_2 concentrations over the last glacial termination. *Science* **291,** 112–114 (2001).
10. Ahn, J. *et al.* A record of atmospheric CO_2 during the last 40,000 years from the Siple Dome, Antarctica ice core. *J. Geophys. Res.* **109,** D13305 (2004).
11. WAIS Divide Project Members. Onset of deglacial warming in West Antarctica driven by local orbital forcing. *Nature* **500,** 440–444 (2013).
12. Brook, E. J., Harder, S., Severinghaus, J., Steig, E. J. & Sucher, C. M. On the origin and timing of rapid changes in atmospheric methane during the last glacial period. *Glob. Biogeochem. Cycles* **14,** 559–572 (2000).
13. Khalil, M. A. K. & Rasmussen, R. A. Sources, sinks, and seasonal cycles of atmospheric methane. *J. Geophys. Res.* **88,** 5131–5144 (1983).
14. Lourantou, A., Chappellaz, J., Barnola, J. M., Masson-Delmotte, V. & Raynaud, D. Changes in atmospheric CO_2 and its carbon isotopic ratio during the penultimate deglaciation. *Quat. Sci. Rev.* **29,** 1983–1992 (2010).
15. Broecker, W. S. Glacial to interglacial changes in ocean chemistry. *Prog. Oceanogr.* **11,** 151–197 (1982).
16. Sigman, D. M., de Boer, A. M. & Haug, G. H. in *Ocean Circulation: Mechanisms and Impacts* (eds Schmittner, A., Chiang, J. C. H. & Hemming, S. R.) 335–349 (American Geophysical Union, 2007).
17. Chiang, J. C. H. & Bitz, C. M. Influence of high latitude ice cover on the marine intertropical convergence zone. *Clim. Dyn.* **25,** 477–496 (2005).
18. Anderson, R. F. *et al.* Wind-driven upwelling in the Southern Ocean and the deglacial rise in atmospheric CO_2. *Science* **323,** 1443–1448 (2009).
19. McManus, J. F., Francois, R., Gherardi, J.-M., Keigwin, L. D. & Brown-Leger, S. Collapse and rapid resumption of Atlantic meridional circulation linked to deglacial climate changes. *Nature* **428,** 834–837 (2004).
20. Schmittner, A. & Galbraith, E. D. Glacial greenhouse-gas fluctuations controlled by ocean circulation changes. *Nature* **456,** 373–376 (2008).
21. Köhler, P., Joos, F., Gerber, S. & Knutti, R. Simulated changes in vegetation distribution, land carbon storage, and atmospheric CO_2 in response to a collapse of the North Atlantic thermohaline circulation. *Clim. Dyn.* **25,** 689–708 (2005).
22. Köhler, P., Knorr, G., Buiron, D., Lourantou, A. & Chappellaz, J. Abrupt rise in atmospheric CO_2 at the onset of the Bølling/Allerød: in-situ ice core data versus true atmospheric signals. *Clim. Past* **7,** 473–486 (2011).
23. Stern, J. V. & Lisiecki, L. E. North Atlantic circulation and reservoir age changes over the past 41,000 years: North Atlantic reservoir age history. *Geophys. Res. Lett.* **40,** 3693–3697 (2013).
24. Toggweiler, J. R., Russell, J. L. & Carson, S. R. Midlatitude westerlies, atmospheric CO_2, and climate change during the ice ages. *Paleoceanography* **21,** PA2005 (2006).
25. Sachs, J. P. & Anderson, R. F. Increased productivity in the subantarctic ocean during Heinrich events. *Nature* **434,** 1118–1121 (2005).
26. Partin, J. W., Cobb, K. M., Adkins, J. F., Clark, B. & Fernandez, D. P. Millenial-scale trends in west Pacific warm pool hydrology since the Last Glacial Maximum. *Nature* **449,** 452–455 (2007).
27. Wu, J., Wang, Y., Cheng, H. & Edwards, L. R. An exceptionally strengthened East Asian summer monsoon event between 19.9 and 17.1 ka BP recorded in a Hulu stalagmite. *Sci. China Ser. Earth Sci.* **52,** 360–368 (2009).
28. Stager, J. C., Ryves, D. B., Chase, B. M. & Pausata, F. S. R. Catastrophic drought in the Afro-Asian monsoon region during Heinrich event 1. *Science* **331,** 1299–1302 (2011).
29. Scholze, M., Knorr, W. & Heimann, M. Modelling terrestrial vegetation dynamics and carbon cycling for an abrupt climatic change event. *Holocene* **13,** 327–333 (2003).
30. Weber, M. E. *et al.* Millennial-scale variability in Antarctic ice-sheet discharge during the last deglaciation. *Nature* **510,** 134–138 (2014).
31. Schilt, A. *et al.* Atmospheric nitrous oxide during the last 140,000 years. *Earth Planet. Sci. Lett.* **300,** 33–43 (2010).
32. Ramaswamy, V. *et al. Climate Change 2001: The Scientific Basis* (eds Houghton, J. T. *et al.*) 349–416 (Cambridge Univ. Press, 2001).

Supplementary Information is available in the online version of the paper.

Acknowledgements This work is supported by the US National Science Foundation (NSF) (grants 0739766-ANT, 1043518-ANT, 1043092-ANT, 0839093-ANT and 1142166-ANT). We appreciate the support of the WAIS Divide Science Coordination Office at the Desert Research Institute (DRI) of Reno, Nevada, and the University of New Hampshire for the collection and distribution of the WAIS Divide ice core and related tasks (NSF grants 0230396, 0440817, 0944348 and 0944266). Additional support for this research came from the NSF Office of Polar Programs through their support of the Ice Drilling Program Office and the Ice Drilling Design and Operations group; the US National Ice Core Laboratory, for curation of the core; Raytheon Polar Services, for logistics support in Antarctica; the 109th New York Air National Guard, for airlift to Antarctica; and the Korea Meteorological Administration Research and Development Program (CATER 2012-7030). We thank T. Alig, J. Edwards and J. Lee for assisting with CO_2 and CH_4 measurements; the DRI ultratrace ice-core lab, including D. Pasteris, M. Sigl and O. Maselli for their contribution to the aerosol records; and I. Fung for discussions and providing software for carbon uptake calculations.

Author Contributions S.A.M. and E.J.B. oversaw and contributed to all aspects of the research, and with T.K.B. designed the project and led the writing of the paper. J.A., M.L.K., J.P.S. and T.S. assisted with and contributed WDC gas measurements. E.J.S. contributed the WDC water isotope data. J.R.M. contributed calcium and hydrogen peroxide concentration measurements. C.B. developed the gas chronology. J.L.R. performed the firn modelling experiments and interpretation. K.C.T. led the field effort that collected the samples. K.M.C., T.J.F., J.R.M., E.J.S., K.C.T. and J.W.C.W. developed the ice chronology and interpretation. All authors discussed the results and contributed input to the manuscript.

Author Information Reprints and permissions information is available at www.nature.com/reprints. The authors declare no competing financial interests. Readers are welcome to comment on the online version of the paper. Correspondence and requests for materials should be addressed to S.A.M. (smarcott@wisc.edu).

METHODS

Measurements of CO_2 were made at Oregon State University, and CH_4 measurements were made at Oregon State and Penn State University. CO_2 measurements were made with a mechanical crushing system using methods described by Ahn *et al.*[33]. Approximately 1,030 measurements were made on ~320 separate depths spanning the time frame of 23,000–9,000 years BP with a median sampling resolution of 25 years. All samples were measured at least in duplicate and one to three times more for some depths. Nitrogen isotope data were used to correct the CO_2 data by 1.0–1.4 p.p.m. for gravitational fractionation. The mean standard error of all measurements was 1.0 p.p.m. A consistent 4 p.p.m. offset between WDC and EPICA Dome C CO_2 concentrations is observed. A similar offset is observed between WAIS Divide and other CO_2 reconstructions[34]. Methane concentrations were measured for approximately 1,100 ice samples from ~580 depths covering 23,000–11,500 years BP (20-year median resolution) using methods described by Mitchell *et al.*[35] at Oregon State University and combined with data measured at Penn State University[11]. Duplicate methane measurements were made on all but fifty samples, and the mean standard error of all measurements made at Oregon State University was 0.8 p.p.b. CO_2 and CH_4 measurements were calibrated using dry standard air with known mole fractions calibrated at the NOAA Earth System Research Laboratory (WMOX2007 scale for CO_2; NOAA04 scale for CH_4).

WAIS Divide timescale. The gas chronology used in this study (WDC06A-7) is based on the layer-counted WDC06A-7 chronology[11]. Gas ages were obtained by subtracting a modelled ice-age/gas-age difference (Δage) from the ice-age timescale[36]. Δage was calculated using a dynamical firn-densification model with heat diffusion. The modelling is constrained by measurements of $\delta^{15}N$ of N_2, a proxy for past firn column thickness[37]. $\delta^{15}N$ was measured on the WAIS Divide ice core (WDC) at the Scripps Institution of Oceanography with a 300-year average resolution (Extended Data Fig. 1b) following procedures outlined elsewhere[38,39]. The air was extracted from ~13 g ice samples using a melt–refreeze technique, and collected on a cold finger at liquid-He temperatures. The samples were analysed on a Thermo Finnigan Delta V dual-inlet mass spectrometer to determine $^{15}N/^{14}N$ of N_2 ($\delta^{15}N$), $^{18}O/^{16}O$ of O_2 ($\delta^{18}O$), $^{32}O_2/^{28}N_2$ ($\delta O_2/N_2$) and $^{40}Ar/^{28}N_2$ ($\delta Ar/N_2$). Routine analytical corrections were made to the data for pressure imbalance and chemical slope, and results were normalized to the La Jolla present-day atmosphere.

We use a dynamical adaptation of the Herron and Langway firn-densification model[40] coupled to a heat diffusion–advection model[41]. We use the present-day convective zone thickness of 3.5 m and a parameterization for surface snow density[42,43]. The forward model requires past temperatures and accumulation rates as inputs, and generates Δage and $\delta^{15}N$ as outputs. Surface temperatures (Extended Data Fig. 1a) are obtained from the $\delta^{18}O$ isotopic composition of the ice[11], with the $\delta^{18}O$–temperature relationship calibrated[11,44,45] to fit observed borehole temperatures. Accumulation rates were obtained in two ways. First, accumulation can be reconstructed from the observed annual layer thickness, corrected for thinning due to ice flow (Extended Data Fig. 1c, black curve). However, the thinning function becomes increasingly uncertain with depth (the CO_2 data presented here were measured over the depth range of 1,700–2,600 m within the 3,405 m-long core). Second, accumulation can be reconstructed from the $\delta^{15}N$ data using a firn-densification inverse model[41]. Using the temperature history, the model determines the accumulation history that optimizes the fit to the $\delta^{15}N$ data by making small adjustments to the thinning function (Extended Data Fig. 1c, red curve). The model fit to the $\delta^{15}N$ data is shown in Extended Data Fig. 1b. We find a good agreement between both accumulation rate reconstructions.

The modelled Δage is shown in Extended Data Fig. 1d (orange curve), where we have used the accumulation rates from the inverse $\delta^{15}N$ method. A sensitivity study in which we varied past convective zone thicknesses, temperature history, dust sensitivity[46] and firn-densification physics[47] shows a 1σ uncertainty in Δage of ~15%. We also calculated Δage using the depth-difference method developed by Parrenin *et al.*[5] (Extended Data Fig. 1d, black curve). This method also suffers from uncertainty in the layer thinning function. Both methods agree within the 1σ uncertainty band. We note that at around 12 kyr BP the WDC site experienced a very sudden and short-lived increase in accumulation rates as inferred from the annual layer thicknesses (Extended Data Fig. 1c). This event is also recorded in the $\delta^{15}N$ as a thickening of the firn column (Extended Data Fig. 1b).

Potential for *in situ* production of CO_2. Prior work in Greenland[8] has demonstrated that CO_2 records can be compromised through *in situ* production when abundant concentrations of calcium carbonate are present. Calcium is delivered to the ice in the form of carbonate dust that blows onto the ice-sheet surface and is buried by subsequent accumulation. Although problems with *in situ* production have never been detected in CO_2 records from Antarctic ice cores, probably because Antarctic sites experience an order of magnitude less calcium carbonate deposition than Greenland[48], each ice core from Antarctica is both geographically unique and affected by distinct atmospheric processes that can deliver various chemical species to the sites. To examine whether abrupt changes in CO_2 in WDC are related to *in situ* production, we compared the non-seasalt component of calcium, which we take as a proxy for terrestrial dust, with the carbon dioxide concentration at times of abrupt change in CO_2 (Extended Data Fig. 2). We find no relationships and note that the non-seasalt Ca also is an order of magnitude lower at WDC than in Greenland ice cores, similar to other ice cores from Antarctica[8,48]. In addition to calcium carbonate, the oxidation of organic compounds can also affect the CO_2 concentration from ice cores[49]. At WDC the concentration of the oxidant H_2O_2 in the upper section of the core (WDC-05A) averaged less than 30 p.p.b.[50,51], which is similar to other values from Antarctic ice cores[52], and does not covary with CO_2 concentrations over the interval from 1,940 to 2,000 m (average 20 p.p.b.) in the deeper section of WDC from where we have data.

Smoothing of the CO_2 record by firn processes. Although it may appear that the WDC and EDC CO_2 records exhibit fundamentally different patterns over short timescales (Extended Data Fig. 3), these differences are expected as a result of the dramatically different conditions at the ice-core sites, which dictate how much smoothing atmospheric gas records experience before being locked into the ice-core record. Temperature and accumulation rates at WDC vary between 233 and 243 K and, respectively, between 0.10 and 0.30 m ice equivalent per year over the deglacial transition. At EDC, in contrast, conditions are colder and dryer, averaging 209 K and 0.015 m yr^{-1}. Because of this, firn models predict that Δage and the age distribution (a measure of smoothing) should be an order of magnitude smaller at WDC than at EDC (Extended Data Fig. 4).

To demonstrate the consistency of the two CO_2 records, we generate a smoothing function for EDC using the OSU firn air model[53] (Extended Data Fig. 5a). The function describes the age distribution of the air in the closed porosity of the ice core, and accounts for gradual bubble closure as ice is advected through the lock-in zone. We then apply this filter to the WDC gas record, using it as a proxy for the true atmospheric history. Because WDC gases experience very little smoothing during bubble trapping, we argue that this is a reasonable assumption (smoothing WDC with a WDC filter does not change the record). The resulting curve agrees well with the EDC CO_2 record[9,14,54] (Extended Data Fig. 5b), supporting the idea that differences between the two records arise because of differences in site conditions and bubble-trapping processes, and reflect no disagreement about the nature of the deglacial rise in atmospheric CO_2.

A consistent 4 p.p.m. offset between WDC and EPICA Dome C CO_2 concentrations is observed in our new deglacial reconstruction after consideration for firn smoothing processes (Extended Data Figs 3 and 5). This offset represents 1–2% of the total concentration measurements and is outside the stated uncertainties for both records. A similar offset of 2–4 p.p.m. has also been observed between WDC and CO_2 reconstructions from Law Dome and EPICA Dronning Maud Land[34], along with a 2 p.p.m. offset between Dronning Maud Land and the South Pole[52]. On the basis of interlaboratory comparisons between Law Dome and WDC[34], the offset between the ice cores is unlikely to result from laboratory methods and represents a real difference between the two ice cores, though the exact nature of the offset still remains to be determined.

Modelling CO_2 pulses and plateaux. Using the WDC CO_2 record as a proxy for the true atmospheric history, we employ a box model of the ocean carbon cycle[55] to explore how a pulse of CO_2 emissions is attenuated and potentially creates a plateau in the concentration record. The model is divided into three boxes: a well-mixed atmosphere, a well-mixed surface ocean mixed layer and a diffusive thermocline/deep ocean. The model does not account for sedimentation of $CaCO_3$ in the ocean. To simulate an abrupt increase in CO_2, we apply a pulse input of 0.5 Pg C yr^{-1} that lasts for 100 years. Following the 100-year pulse, the model simulates a slow ocean uptake over the next 1,500 years (Extended Data Fig. 6). Although this model is not designed to simulate the entire CO_2 variability in the WDC record, this simple simulation suggests (but does not require) that the three abrupt CO_2 rises at 16.3, 14.8 and 11.7 kyr ago could represent brief injections of CO_2 into the atmosphere that are superimposed on a longer-term increase, with the plateau that follows each of the abrupt rises explained by the drawdown of the additional carbon in the atmosphere into the ocean.

Köhler *et al.*[21] performed a similar experiment using a more comprehensive carbon cycle box model to describe an abrupt CO_2 change at the onset of the Bølling. Using similar modelled pulses of CO_2, they also reproduced the abrupt CO_2 features. They concluded that the magnitude of the CO_2 change could have been as high as 30 p.p.m. for a 2.5 Pg yr^{-1} injection of carbon into the atmosphere after considering smoothing of the atmospheric signal in the firn at EDC. Unlike the low-accumulation site at EDC, however, the high-accumulation WDC site provides a CO_2 record that has experienced very little firn smoothing (see Methods section on the WAIS Divide timescale), and provides a much closer approximation of the true atmospheric history. Therefore, we conclude that if there were a pulse input of CO_2 its magnitude and duration would be of the order of 0.5 Pg C yr^{-1} and would last for 100 years.

Breakpoint determination. To provide an objective means for determining the timing and duration of the CO_2 and CH_4 transitions across the last deglaciation, we employed the functions Breakfit[56] and Rampfit[57]. For the three abrupt jumps in CO_2, both the timing and duration of the changes were quantified (Extended Data Table 1) using the Rampfit[57] function with a 500-year search window. For each, the same seed generator number (200) was used, and 200 bootstrap (wild) iterations were performed to determine the uncertainties. For the CO_2 and CH_4 transitions at the start of the deglaciation and beginning of the Younger Dryas, the Breakfit[56] function was used to determine the timing of the transitions. The window length for each was 1,000 years and the same seed number (200) and bootstrap number (200) were used to quantify the timing uncertainty.

33. Ahn, J., Brook, E. J. & Howell, K. A high-precision method for measurement of paleoatmospheric CO_2 in small polar ice samples. *J. Glaciol.* **55,** 499–506 (2009).
34. Ahn, J. *et al.* Atmospheric CO_2 over the last 1000 years: a high-resolution record from the West Antarctic Ice Sheet (WAIS) Divide ice core. *Glob. Biogeochem. Cycles* **26,** GB2027 (2012).
35. Mitchell, L. E., Brook, E. J., Sowers, T., McConnell, J. R. & Taylor, K. Mulidecadal variability of atmospheric methane, 1000-1800 C.E. *J. Geophys. Res.* **116,** G02007 (2011).
36. Schwander, J. & Stauffer, B. Age difference between polar ice and the air trapped in its bubbles. *Nature* **311,** 45–47 (1984).
37. Sowers, T., Bender, M., Raynaud, D. & Korotkevich, Y. S. $\delta^{15}N$ of N_2 in air trapped in polar ice: a tracer of gas transport in the firn and a possible constraint on ice age-gas age difference. *J. Geophys. Res.* **97,** 15683–15697 (1992).
38. Sowers, T., Bender, M. & Raynaud, D. Elemental and isotopic composition of occluded O_2 and N_2 in polar ice. *J. Geophys. Res.* **94,** 5137–5150 (1989).
39. Petrenko, V. V., Severinghaus, J. P., Brook, E. J., Reeh, N. & Schaefer, H. Gas records from the West Greenland ice margin covering the Last Glacial Termination: a horizontal ice core. *Quat. Sci. Rev.* **25,** 865–875 (2006).
40. Herron, M. M. & Langway, C. C. Firn densification: an empirical model. *J. Glaciol.* **93,** 373–383 (1980).
41. Rasmussen, S. O. *et al.* A first chronology for the North Greenland Eemian Ice Drilling (NEEM) ice core. *Clim. Past* **9,** 2713–2730 (2013).
42. Kaspers, K. A. *et al.* Model calculations of the age of firn air across the Antarctic continent. *Atmos. Chem. Phys.* **4,** 1365–1380 (2004).
43. Battle, M. O. *et al.* Controls on the movement and composition of firn air at the West Antarctic Ice Sheet Divide. *Atmos. Chem. Phys.* **11,** 18633–18675 (2011).
44. Cuffey, K. M. & Glow, G. D. Temperature, accumulation, and ice sheet elevation in central Greenland through the last deglacial transition. *J. Geophys. Res.* **102,** 26383–26396 (1997).
45. Steig, E. J. *et al.* Recent climate and ice-sheet change in West Antarctica compared to the past 2000 years. *Nature Geosci.* **6,** 372–375 (2013).
46. Hörhold, M. W. *et al.* On the impact of impurities on the densification of polar firn. *Earth Planet. Sci. Lett.* **325–326,** 93–99 (2012).
47. Barnola, J. M., Pimienta, P., Raynaud, D. & Korotkevich, Y. S. CO_2–climate relationship as deduced from the Vostok ice core: a reexamination based on new measurements and on a reevaluation of the air dating. *Tellus B* **43,** 83–90 (1991).
48. Legrand, M. R. & Delmas, R. J. Soluble impurities in four Antarctic ice cores over the last 30,000 years. *Ann. Glaciol.* **10,** 116–120 (1988).
49. Tschumi, J. & Stauffer, B. Reconstructing past atmospheric CO_2 concentration based on ice-core analyses: open questions due to in situ production of CO_2 in the ice. *J. Glaciol.* **46,** 45–53 (2000).
50. Sofen, E. D. *et al.* WAIS Divide ice core suggests sustained changes in the atmospheric formation pathways of sulfate and nitrate since the 19th century in the extratropical Southern Hemisphere. *Atmos. Chem. Phys. Discuss.* **13,** 23089–23138 (2013).
51. Lamarque, J.-F., McConnell, J. R., Shindell, D. T., Orlando, J. J. & Tyndall, G. S. Understanding the drivers for the 20th century change of hydrogen peroxide in Antarctic ice-cores. *Geophys. Res. Lett.* **38,** L04810 (2011).
52. Siegenthaler, U. *et al.* Supporting evidence from the EPICA Dronning Maud Land ice core for atmospheric CO_2 change during the past millenium. *Tellus B* **57,** 51–57 (2005).
53. Buizert, C. *et al.* Gas transport in firn: multiple-tracer characterisation and model intercomparison for NEEM, Northern Greenland. *Atmos. Chem. Phys. Discuss.* **11,** 15975–16021 (2011).
54. Lemieux-Dudon, B. *et al.* Consistent dating of Antarctica and Greenland ice cores. *Quat. Sci. Rev.* **29,** 8–20 (2010).
55. Oeschger, H., Siegenthaler, U., Schotterer, U. & Gugelmann, A. A box diffusion model to study the carbon dioxide exchange in nature. *Tellus* **27,** 168–192 (1975).
56. Mudelsee, M. Break function regression: a tool for quantifying trend changes in climate time series. *Eur. Phys. J. Spec. Top.* **174,** 49–63 (2009).
57. Mudelsee, M. Ramp function regression: a tool for quantifying climate transitions. *Comput. Geosci.* **26,** 293–307 (2000).
58. Veres, D. *et al.* Antarctic ice core chronology (AICC2012): an optimized multi-parameter and multi-site dating approach for the last 120 thousand years. *Clim. Past* **9,** 1733–1748 (2013).
59. Bazin, L. *et al.* An optimized multi-proxies, multi-site Antarctic ice and gas orbital chronology (AICC2012): 120-800 ka. *Clim. Past* **9,** 1715–1731 (2013).

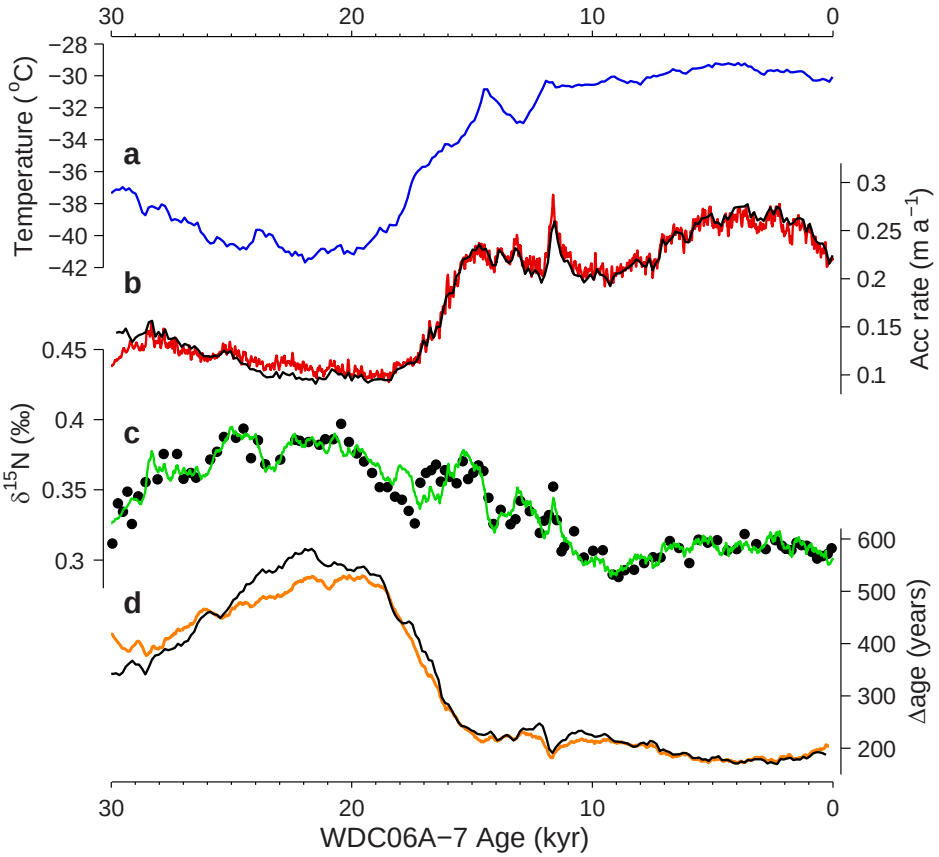

Extended Data Figure 1 | $\delta^{15}N$ and the ice-age/gas-age difference for the WDC. **a**, Borehole calibrated surface temperature reconstruction derived from $\delta^{18}O$ measurements from the ice[1]. **b**, Accumulation rates reconstructed with the firn-densification inverse model (red curve) and from layer thickness observations (black curve). **c**, $\delta^{15}N$-N_2 data for the upper 2,800 m (black dots) with model fit (green curve). **d**, Modelled age using firn-densification model (orange curve) and Δage estimate using the depth-difference technique from Parrenin *et al.*[5] (black curve).

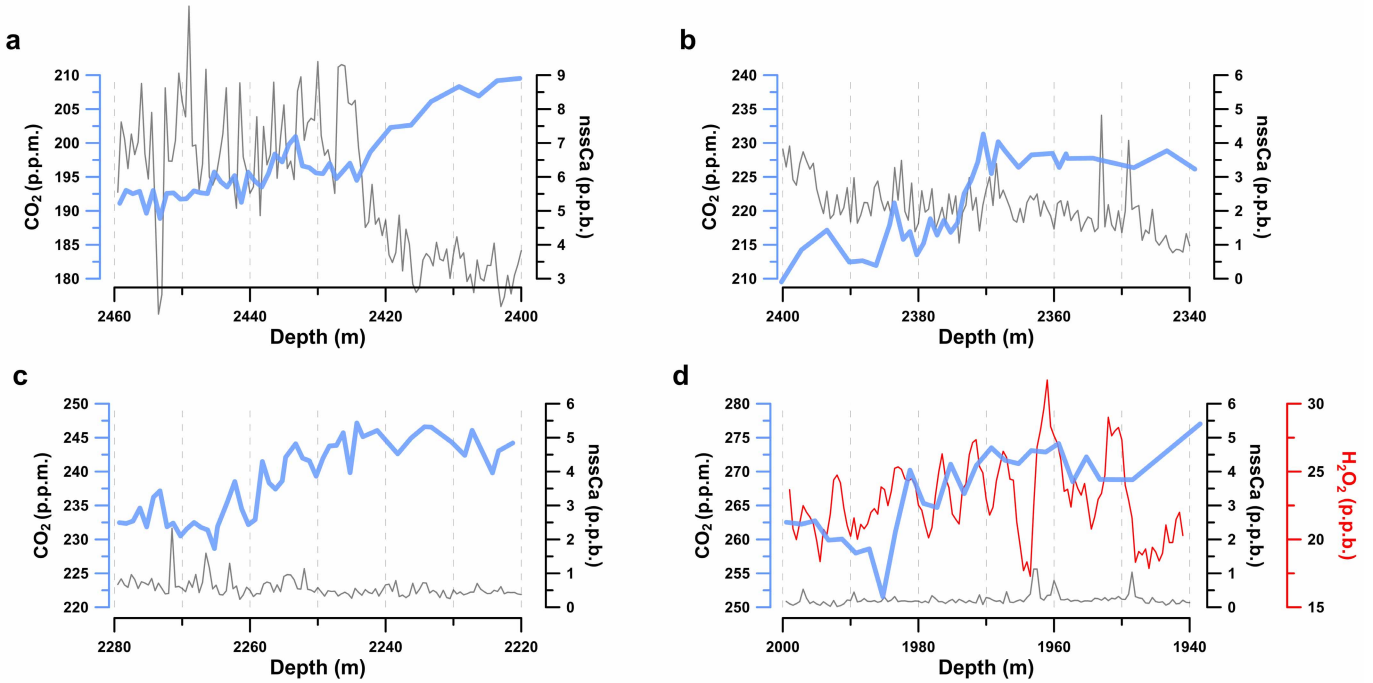

Extended Data Figure 2 | CO_2 concentrations and elemental data for WDC. WDC CO_2 concentrations (blue) plotted against non-seasalt calcium (nssCa) concentrations (black) and hydrogen peroxide (H_2O_2, red) at multiple depths in the core where we observe abrupt changes in carbon dioxide. Hydrogen peroxide concentrations have been smoothed (2 m centred average) from original data to improve clarity.

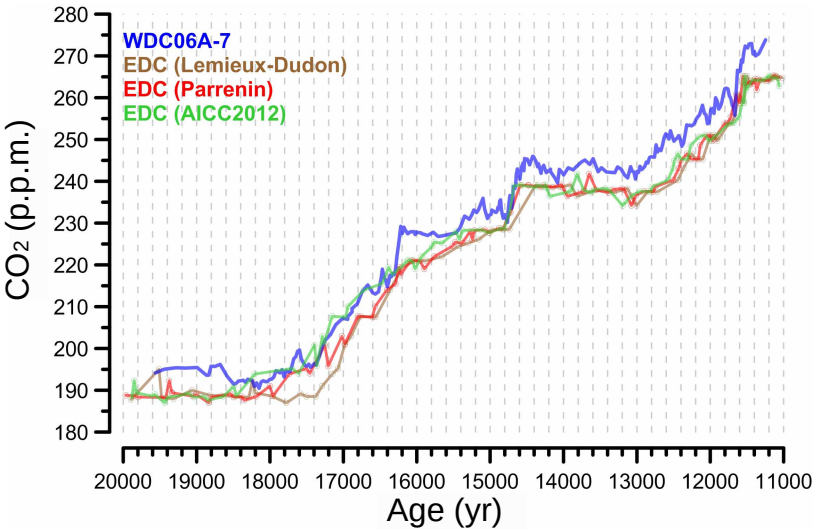

Extended Data Figure 3 | CO_2 concentrations for WDC and EDC. WDC CO_2 concentrations on layer-counted (blue; 5-point weighted average) timescale and EPICA Dome C (EDC) CO_2 concentrations on the Lemieux-Dudon *et al.*[9,14,54] (brown), Parrenin *et al.*[5] (red) and Antarctic ice-core chronology[58,59] (AICC2012; green) timescales.

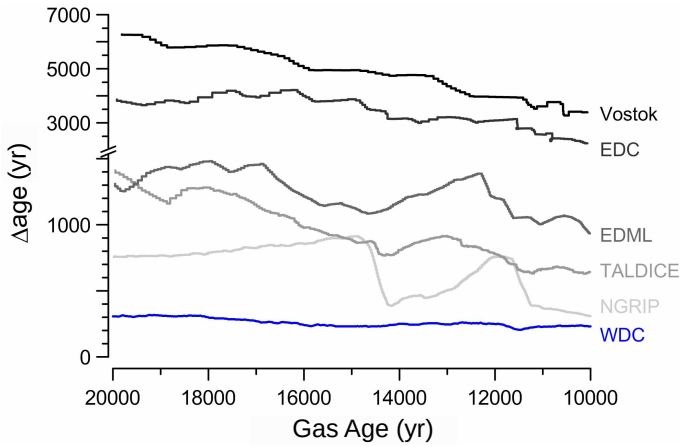

Extended Data Figure 4 | Calculated Δage offsets across the last deglacial termination for five ice cores from Antarctica and Greenland, compared with WDC. EDML, EPICA Dronning Maud Land; TALDICE, Talos Dome Ice; NGRIP, North Greenland Ice Project. Ice-core data from refs 58, 59.

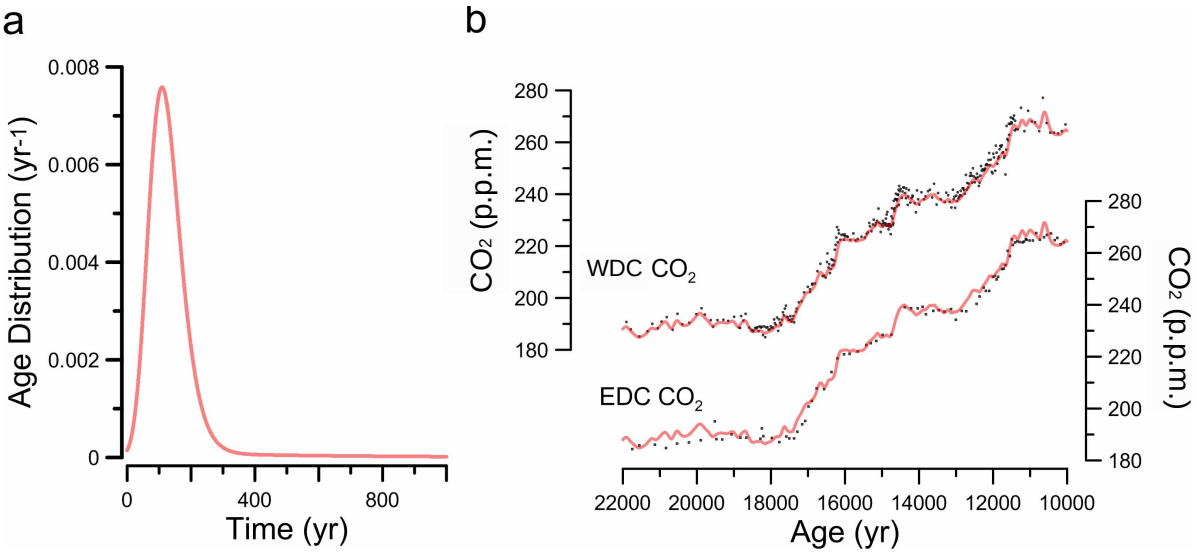

Extended Data Figure 5 | Firn smoothing functions applied to CO_2 data from WDC and EDC. **a**, The red line is the Green's function (smoothing function) produced by a firn model using an assumed EDC accumulation rate of 0.015 m yr^{-1} and a temperature of 209 K. **b**, CO_2 data from WDC (dots) and EDC (dots) plotted against artificially smoothed CO_2 data from WDC using the EDC firn smoothing function (red line in both plots). WDC data have been systematically lowered by 4 p.p.m. for direct comparison with EDC.

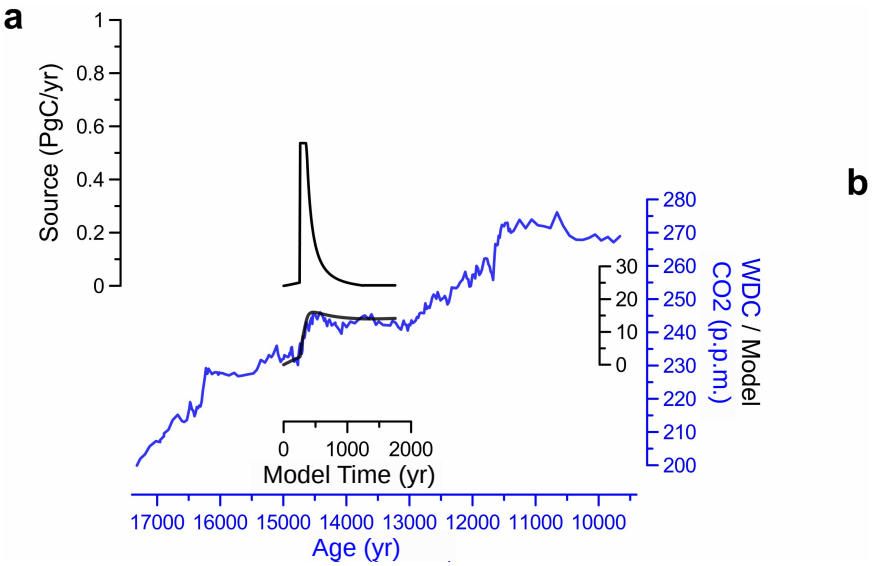

Extended Data Figure 6 | Simple box model source history and atmospheric CO_2 response compared to measured data from WDC. **a**, Applied source history used in the modelling experiment. **b**, Atmospheric CO_2 record from WDC (5-point weighted average; blue) and the model derived atmospheric history (black). Box model from ref. 55.

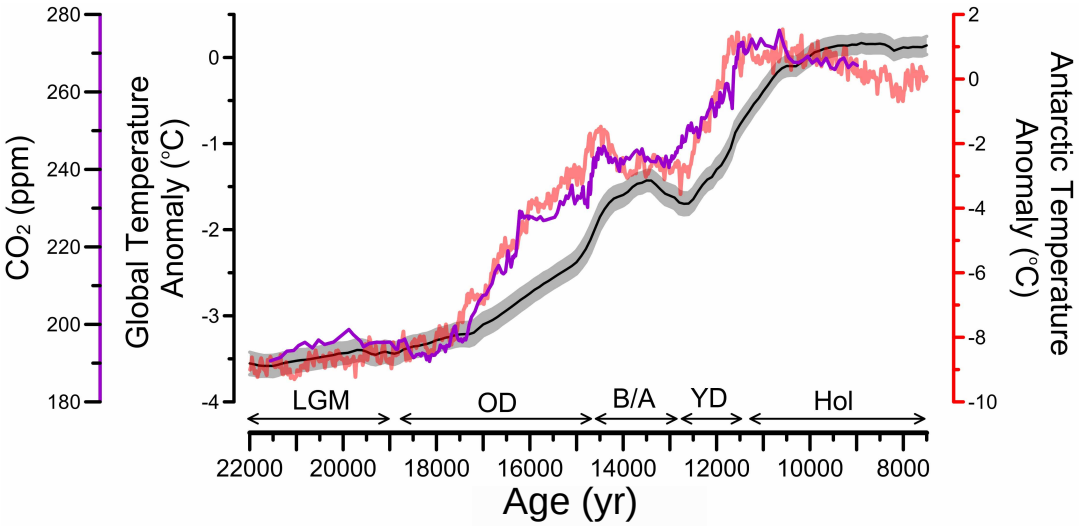

Extended Data Figure 7 | CO_2 concentrations and temperature reconstructions for the last deglaciation. WDC CO_2 concentrations (purple; 5-point weighted average), a global temperature reconstruction[2] (black; grey band is 1σ uncertainty envelope), and an Antarctic temperature stack based on stable isotopes from East Antarctic ice cores[5] (red).

Extended Data Table 1 | Timing of five abrupt transitions in CO_2 and CH_4 during the last termination

Rampfit (CO_2)	Search Window (yrs BP)	Breakpoint 1 (yrs BP)	Breakpoint 2 (yrs BP)	Duration (yrs BP)
"16.3ka" rise	16,500 - 16,000	16,200±20	16,300±20	100±30
"14.8ka" rise	14,900 - 14,400	14,560±30	14,760±30	200±40
"11.7ka" rise	11,900 - 11,400	11,550±40	11,650±30	100±50
Breakfit (CO_2 & CH_4)	Search Window (yrs BP)	Breakpoint CO_2 (yrs BP)	Breakpoint CH_4 (yrs BP)	
"18.1ka"	18,500 - 17,500	18,140±80	17,820±60	
"13.0ka"	13,500 - 12,500	13,020±40	13,010±170	

Uncertainties are 1σ.